Goldberg–Shprintzen syndrome protein KIF1BP is a CITK interactor implicated in cytokinesis

Goldberg-Shprintzen syndrome protein KIF1BP is a CITK interactor implicated in cytokinesis.

Gianmarco Pallavicini[1,2*], Marta Gai[3], Giorgia Iegiani[1,2], Gaia Elena Berto[1,2], Annie Adrait[4], Yohann Couté[4] and Ferdinando Di Cunto[1,2*]

1. Neuroscience Institute Cavalieri Ottolenghi, Turin, Italy.

2. Department of Neuroscience 'Rita Levi Montalcini', University of Turin, Italy.

3. Department of Molecular Biotechnology and Health Sciences, University of Turin, Italy.

4. Univ. Grenoble Alpes, CEA, INSERM, IRIG, BGE, 38000 Grenoble, France.

*Correspondence: gianmarco.pallavicini@unito.it; ferdinando.dicunto@unito.it

Abstract

Goldberg-Shprintzen disease (GOSHS) is a rare microcephaly syndrome accompanied by intellectual disability, dysmorphic facial features, peripheral neuropathy and Hirschsprung disease. It is associated with recessive mutations in the gene encoding kinesin family member 1-binding protein (*KIF1BP*). KIF1BP regulates axon microtubules dynamics, kinesin attachment and mitochondrial biogenesis, but it is not clear how its loss could lead to microcephaly. We identified KIF1BP in the interactome of Citron Kinase (CITK), a protein produced by primary hereditary microcephaly 17 (*MCPH17*) gene. CITK loss induces DNA damage, apoptosis, imbalanced division of neural progenitors and cytokinesis failure. In this report, we showed that KIF1BP and CITK interact under physiological conditions in mitotic cells. Furthermore, KIF1BP is enriched at the midbody ring and, likewise CITK, is required for cytokinesis. Moreover, KIF1BP loss decreases microtubule stability at intercellular bridge and leads to abnormal localization of Chromosome Passenger Complex (CPC). These data suggest that GOSHS microcephaly could be produced by CITK-dependent mechanisms, including cytokinesis failure.

Keywords: KIF1BP, KBP, KIAA1279, Citron kinase, cytokinesis, abscission, AURKB, AuroraB, INCENP

Introduction

Congenital microcephaly (CM) is a heterogeneous group of disorders, characterized by reduced head circumference at birth, to at least 3 standard deviations below the mean (Passemard et al., 2013; Woods and Parker, 2013). CM can be the result of non-genetic conditions, such as viral infections and toxic exposure, or it can be generated by rare genetic disorders (Passemard et al., 2013). CM is also one of the leading features of complex syndromes, comprising structural brain abnormalities, seizures, palsy, ataxia, short stature, skeletal abnormalities and cancer predisposition (Abuelo, 2007; Passemard et al., 2013; Woods and Parker, 2013). At the cellular level, CM is characterized by reduced expansion of neural progenitors, anticipated cell cycle's exit and/or increased apoptosis, resulting in reduced number of neuronal and glial cells.

Primary hereditary microcephaly (MCPH) is the simplest form of genetic CM, in which brain size reduction is accompanied by grossly normal brain architecture and mild to moderate intellectual disability (Mahmood et al., 2011; Passemard et al., 2013). Functional analysis of proteins encoded by MCPH genes has revealed that they are involved in different biological processes, such as centriole biogenesis, centrosome dynamics, centromere and kinetochore function, transmembrane or intracellular transport, Wnt signaling, autophagy, apical polarity complex localization, DNA replication and repair and cytokinesis (Boonsawat et al., 2019; Jayaraman et al., 2018; Naveed et al., 2018; Passemard et al., 2013; Zhou et al., 2020). Microtubules are crucial for many of these functions and important roles of microtubules are increasingly being recognized in phenotypes of cells with reduced function of MCPH genes (Gai et al., 2016; Jin et al., 2017; Pagnamenta et al., 2019; Pilaz et al., 2016; Sgrò et al., 2016).

CITK is the main product of the *MCPH17* (*CIT*) gene (Harding et al., 2016; Li et al., 2016). It controls microtubules' dynamics (Gai et al., 2016; Sgrò et al., 2016) and its loss leads to many cellular phenotypes associated to MCPH, including abnormal spindle orientation,

DNA damage, apoptosis and cytokinesis failure (Bassi et al., 2011; Bianchi et al., 2017b; Gai et al., 2011; Sgrò et al., 2016). CITK is a well know regulator of the final stage of cytokinesis, called abscission, that is the final cut of the microtubule bridge that links the two daughter cells (D'Avino, 2017). After cleavage furrow ingression, the two cells form a structure called midbody. This is divided in a central region called midbody core, around which several proteins form a midbody ring. The flanking regions of this bulge are called midbody arms (Hu et al., 2012). CITK localizes at midbody ring and is important to maintain midbody architecture and stability through multiple mechanisms (Bianchi et al., 2017a; Capalbo et al., 2019; D'Avino, 2017; Dema et al., 2018). In particular, CITK contributes to midbody maturation by bridging at midbody arms Chromosomal Passenger Complex (CPC) proteins, such as Aurora B (AURKB) and INCENP, with midbody ring kinesins MKLP1, KIF14 and KIF23 (McKenzie et al., 2016). This complex is required for midbody organization and abscission.

Goldberg-Shprintzen disease (GOSHS, OMIM 609460) is a rare microcephaly syndrome characterized by intellectual disability, dysmorphic facial features, peripheral neuropathy as well as Hirschsprung disease (Brooks et al., 2005; Dafsari et al., 2015; Drévillon et al., 2013; Valence et al., 2013). Recessive mutations in the gene encoding KIF1BP are associated with GOSHS (Brooks et al., 2005). Consistently, KIF1BP knockout mice show a small flat head, among other neurological features (Hirst et al., 2017). KIF1BP has been implicated in organization of neuronal microtubules, as well as axonal growth and maintenance (Drerup et al., 2016; Kevenaar et al., 2016; Lyons et al., 2008). Moreover, it has a direct role in mitochondria distribution (Wozniak et al., 2005) and mitochondrial biogenesis in mouse embryonic stem cells (Donato et al., 2017). Finally, KIF1BP regulates chromosomes congression and alignment during mitosis, by buffering KIF15 and KIF18 kinesins (Brouwers et al., 2017; Malaby et al., 2019). Nevertheless, it is not understood how KIF1BP loss could generate microcephaly.

To better understand how CITK may affect microtubules, we used affinity chromatography, followed by mass spectrometry (MS)-based proteomics to map its binding partners. Notably, this strategy highlighted the association of CITK with KIF1BP. Therefore, we explored more in details the relationship of these two proteins. Our result highlight a functional involvement of KBP in cytokinesis.

Results

Identification of new CITK partners by affinity chromatography coupled to MS-based proteomics.

To identify new CITK partners, we resorted to an interactomic approach. We overexpressed in 293-T cells the Cherry protein (control) and the following Cherry -tagged versions of CITK: wild type (CITK), K126A inactive mutant (CITKD) (Di Cunto et al., 1998) and CITN, a natural product of the *CIT* gene completely lacking the kinase domain (Camera et al., 2003). The reason for using kinase-inactive or kinase-lacking proteins was that they may be more efficient to trap in stable complexes CITK interactors, especially those that are direct substrates of its kinase activity (Macías-Silva et al., 1996). Overexpressed proteins were purified by affinity chromatography (Fig. S1) and SDS-PAGE of immune-complexes revealed interactors in the kinase defective CITK lanes (Fig. S1). MS-based proteomic analysis of the co-immunoprecipitation eluates identified 53 different proteins strongly enriched with at least one of the version of CITK, compared to negative control (Tab. S1), half of which were common to the three baits. Several of these proteins were common to those identified in a previous study (McKenzie et al., 2016). These included cytokinesis players previously connected to CITK function, such as KIF14 and KIF23 (Bassi et al., 2013), ANLN (Gai et al., 2011), RACGAP1 (Chalamalasetty et al., 2006) and PPP1R12A (MYPT1) (Capalbo et al., 2019; Kawano et al., 1999). The results strongly validate our biochemical approach. Interestingly, a majority of the identified proteins were significantly enriched or exclusively detected in the immunoprecipitate of

catalytically inactive bait (CITKD). Intriguingly, one of the proteins reliably identified only in the CITKD immunoprecipitation was the kinesin-binding protein KIF1BP.

Validation of the KIF1BP/CITK interaction.

We evaluated more in detail the interaction of CITK with KIF1BP, since this protein may regulate different CITK-interacting kinesins, such as KIF14 and KIF23 (Kevenaar et al., 2016); moreover, *KIF1BP* is involved in the microcephaly syndrome GOSHS (Brooks et al., 2005; Valence et al., 2013) suggesting that a functional interaction with CITK could be relevant for the molecular mechanisms common to this disease and MCPH.

We confirmed the presence of endogenous KIF1BP in immunocomplexes of overexpressed Cherry-CITK and Cherry-CITKD, by performing western blot analysis with KIF1BP-specific antibodies (Fig. 1A). Consistent with MS results, the amount of KIF1BP co-immunoprecipitated with Cherry -CITKD was higher than with Cherry-CITK (Fig. 1A). The binding was not dependent on using the Cherry epitope, since similar results were obtained by immunoprecipitating overexpressed active and dead CITK fused to a MYC epitope (Fig. 1B). Reciprocal co-immunoprecipitation was obtained in 293 cells, co-transfected with MYC-tagged CITK and FLAG-tagged KIF1BP, performing IP with anti-FLAG antibodies. (Fig. 1C). Even the reciprocal co-immunoprecipitation assay revealed increased association of KIF1BP with CITKD, as compared to the kinase-active protein (Fig. 1C). Importantly, we detected co-immunoprecipitation of endogenous CITK and KIF1BP, from lysates of HeLa cells synchronized in mitosis (Fig. 1D), when CITK is expressed at higher levels.

These data demonstrate that KIF1BP and CITK can be part of a complex under physiological conditions and show that CITK catalytic activity may influence association strength.

KIF1BP is required for cytokinesis.

KIF1BP is required for the alignment of chromosomes at the metaphase plate and for the assembly of stable kinetochore fibers of correct length (Brouwers et al., 2017; Malaby et al., 2019). Considering the KIF1BP/CITK interaction (Fig. 1), we asked whether KIF1BP may also share a role with CITK in cytokinesis.

Immunofluorescence analysis of wild type HeLa cells revealed that, in late cytokinesis, KIF1BP associates with the midbody (Fig 2A). In particular, KIF1BP is enriched at the midbody ring, where also CITK reaches its highest concentration (Bassi et al., 2013). This staining disappeared in cells treated with specific siRNA against KIF1BP (Fig 2A). The specific association of KIF1BP with the midbody was further confirmed by analyzing the localization of an N-terminal GFP-fusion protein, overexpressed in HeLa cells (Fig. 2B).

To assess whether KIF1BP plays a functional role in abscission, we tested the effects of KIF1BP knockdown (Fig. 2C) in proliferating HeLa cells. Loss of KIF1BP leads to significant increase of binucleated cells (Fig. 2D), which is suggestive of cytokinesis failure. Dynamic microscopy of mitotic cells division showed that KIF1BP-depleted cells display significant delay in mitosis (data not shown), as previously reported in literature (Brouwers et al., 2017; Malaby et al., 2019). In addition, they also displayed increased frequency of cytokinesis failure (see supplementary movies 1 and 2). In particular, KIF1BP knockdown cells displayed the same phenotype as CITK loss of function: the midbody forms normally but cytokinesis fails afterwards (Fig. 2E-F), with the two daughter cells fusing back together and forming a binucleated cell (Bassi et al., 2013; Gai et al., 2011).

We then tested whether KIF1BP localization was dependent on CITK, by immunostaining HeLa cells after CITK knockdown (Fig. 3A). Interestingly, quantitative analysis revealed that KIF1BP midbody staining was not decreased after CITK loss. On the contrary, it was slightly but significantly increased (Fig. 3B). Likewise, KIF1BP depletion did not affect CITK levels and localization (Fig. 3C-D).

These data show that both KIF1BP and CITK localize at the midbody and that KIF1BP is required for cell division after midbody formation as well as CITK (D'Avino, 2017). Nevertheless, the localization of the two proteins is not interdependent.

KIF1BP is required for midbody microtubules stability and CPC midbody localization.

Since CITK influences midbody architecture and stability by modulating microtubule dynamics and CPC localization (McKenzie et al., 2016; Sgrò et al., 2016), we wondered whether KIF1BP has similar function in cytokinesis.

First, we measured the ratio of acetylated versus tyrosinated-tubulin at the midbody, to assess whether KIF1BP is important for stabilizing midbody microtubules. Indeed, it is known that stable microtubules have higher levels of acetylated tubulin (Janke and Montagnac, 2017). KIF1BP knockdown cells showed lower levels of acetylated tubulin at the midbody bridge, as compared to control cells (Fig. 4A-B). Then, we analyzed whether the localization of the CPC proteins, was also compromised by KIF1BP RNAi (Fig. 4C-D). In control cells, AURKB is enriched in the midbody arms (Fig. 4C). After KIF1BP knockdown, AURKB showed strongly reduced levels at the midbody, and failed to form the two distinct bands in about 40% of divisions (Fig. 4C-D). Similarly, the midbody signal of INCENP was reduced in KIF1BP knockdown telophases (Fig. 4E-F). In addition, after KIF1BP knockdown, INCENP localized mostly in the midbody core, instead of its normal localization at the midbody arms (Fig. 4E-F).

These results showed that KIF1BP plays the same role as CITK for midbody organization, regulating both microtubule stability and CPC components localization.

Discussion

KIF1BP loss leads to GOSHS syndrome, which is characterized by dysmorphic facial features and multiple alterations of the central and peripheral nervous system. (Brooks et al., 2005; Dafsari et al., 2015; Drévillon et al., 2013; Valence et al., 2013). In this report we

provided new molecular insight about how KIF1BP loss may lead to reduced brain size. We found that KIF1BP can be physically associated with CITK, not only upon overexpression but also at the endogenous protein levels reached by mitotic cells. Previous studies showed that KIF1BP plays a mitotic role before anaphase, promoting chromosomes' congression and alignment (Brouwers et al., 2017; Malaby et al., 2019). Starting from KIF1BP/CITK co-immunoprecipitation, we demonstrated that KIF1BP is also important to complete cytokinesis. In particular, the cytokinesis phenotypes produced by CITK (Gai et al., 2011) or KIF1BP RNAi (Fig. 3C and Supplemental movie 2) are the same, with normal cleavage furrow ingression, apparently normal midbody formation, frequently ending with bridge re-opening and generation of binucleated cells (Fig. 3D). Consistent with this phenotype, both CITK and KIF1BP are strongly enriched at midbody ring, suggesting that they may interact to control abscission.

Previous studies clarified that CITK associates with microtubules (Bassi et al., 2011; Eda et al., 2001), promotes microtubules' stabilization (Sgrò et al., 2016), interacts with kinesins KIF14 and MLKP1 as well as microtubule bundling protein PRC1 (Bassi et al., 2013). The finding that immunocomplexes formed by inactive CITK contain increased levels of three tubulin subunits and KIF1BP (Table S1) suggests that CITK activity may control microtubules dynamics and may also impinge on KIF1BP localization. Accordingly, CITK depletion by RNAi leads to increased levels of KIF1BP at the midbody (Fig. 2C), while KIF1BP loss has no effect on CITK midbody localization. These results support the existence of an epistatic relationship, suggesting that CITK my act upstream of KIF1BP. However, they also exclude that CITK may do so by promoting KIF1BP midbody recruitment. Interestingly, we found that KIF1BP is required to concentrate Chromosomal Passenger Complex (CPC) proteins Aurora-B (AURKB) and INCENP in the midbody arms, as well as to exclude them from midbody core (Fig. 4). This result is very interesting considering the previous identification of a cross-regulatory loop between AURKB and

CITK. The latter is crucial for the orderly arrangement at the midbody of many proteins, including kinesins KIF23 and KIF14. (Bassi et al., 2013; McKenzie et al., 2016) that are also KIF1BP interactors (Kevenaar et al., 2016). Elucidation of the molecular details underlying the dynamic interactions between all these proteins will be an interesting subject for future studies. In particular, a better clarification of all the phosphorylation events controlled by CITK will be crucial, because kinase-inactivating mutations are sufficient to produce severe microcephaly in humans (Harding et al., 2016; Li et al., 2016). Although the best understood function of CITK is abscission control (Bassi et al., 2011; Dema et al., 2018; Gai et al., 2011), it is not excluded that the CITK/KIF1BP interplay may regulate other microcephaly-relevant phenomena. Analysis of cellular and animal models of MCPH17 revealed that CITK is required for normal spindle positioning, which may impinge on asymmetric division (Gai et al., 2016) and prevents the accumulation of DNA double strand breaks, which is critical for p53-dependent apoptosis (Bianchi et al., 2017b). KIF1BP could cooperate with CITK also in these cases. Finally, besides contributing to a better understanding of microcephaly, a deeper elucidation of the KIF1BP/CITK interplay could also provide insight for developing new anti-tumor strategies, considering the anti-tumoral effects determined by CITK inactivation in epithelial tumors (Fu et al., 2011; Meng et al., 2019) and medulloblastoma (Pallavicini et al., 2018, 2020).

Acknowledgements

This work was mainly supported by Associazione Italiana per la Ricerca sul Cancro (AIRC) with grants IG17527 and IG23341 to F. Di Cunto. G. Pallavicini was supported by a fellowship from AIRC. The contribution of University of Torino ex-60% fund to F. Di Cunto is also gratefully acknowledged. Proteomic experiments were partly supported by the ProFI grant (ANR-10-INBS-08-01). We also thank Valerio Donato and Michele Pagano, from New York University, for the plasmids kindly supplied.

Author contributions

GP and FDC conceived, planned and co-directed the project, wrote and edited the manuscript. GP, MG, GI, GEB executed most experiments and analyzed data; AA and YC performed the MS analysis and analyzed the corresponding data;; FDC and GP acquired funding.

References

Abuelo, D. 2007. Microcephaly syndromes. *Semin. Pediatr. Neurol.* 14:118–127. doi:10.1016/j.spen.2007.07.003.

Bassi, Z.I., M. Audusseau, M.G. Riparbelli, G. Callaini, and P.P. D'Avino. 2013. Citron kinase controls a molecular network required for midbody formation in cytokinesis. *Proc. Natl. Acad. Sci.* 110:9782–9787. doi:10.1073/pnas.1301328110.

Bassi, Z.I., K.J. Verbrugghe, L. Capalbo, S. Gregory, E. Montembault, D.M. Glover, and P.P. D'Avino. 2011. Sticky/Citron kinase maintains proper RhoA localization at the cleavage site during cytokinesis. *J. Cell Biol.* 195:595–603. doi:10.1083/jcb.201105136.

Bianchi, F.T., M. Gai, G.E. Berto, and F. Di Cunto. 2017a. Of rings and spines: The multiple facets of Citron proteins in neural development. *Small GTPases*. 1–9. doi:10.1080/21541248.2017.1374325.

Bianchi, F.T., C. Tocco, G. Pallavicini, Y. Liu, F. Vernì, C. Merigliano, S. Bonaccorsi, N. El-Assawy, L. Priano, M. Gai, G.E. Berto, A.M.A. Chiotto, F. Sgrò, A. Caramello, L. Tasca, U. Ala, F. Neri, S. Oliviero, A. Mauro, S. Geley, M. Gatti, and F. Di Cunto. 2017b. Citron Kinase Deficiency Leads to Chromosomal Instability and TP53-Sensitive Microcephaly. *Cell Rep.* 18:1674–1686. doi:10.1016/j.celrep.2017.01.054.

Boonsawat, P., P. Joset, K. Steindl, B. Oneda, L. Gogoll, S. Azzarello-Burri, F. Sheth, C. Datar, I.C. Verma, R.D. Puri, M. Zollino, R. Bachmann-Gagescu, D. Niedrist, M. Papik, J. Figueiro-Silva, R. Masood, M. Zweier, D. Kraemer, S. Lincoln, L. Rodan, Undiagnosed Diseases Network (UDN), S. Passemard, S. Drunat, A. Verloes, A.H.C. Horn, H. Sticht, R. Steinfeld, B. Plecko, B. Latal, O. Jenni, R. Asadollahi, and A. Rauch. 2019. Elucidation of the phenotypic spectrum and genetic landscape in primary and secondary microcephaly. *Genet. Med. Off. J. Am. Coll. Med. Genet.* 21:2043–2058. doi:10.1038/s41436-019-0464-7.

Bouyssié, D., A.-M. Hesse, E. Mouton-Barbosa, M. Rompais, C. Macron, C. Carapito, A. Gonzalez de Peredo, Y. Couté, V. Dupierris, A. Burel, J.-P. Menetrey, A. Kalaitzakis, J. Poisat, A. Romdhani, O. Burlet-Schiltz, S. Cianférani, J. Garin, and C. Bruley. 2020. Proline: an efficient and user-friendly software suite for large-scale proteomics. *Bioinforma. Oxf. Engl.* 36:3148–3155. doi:10.1093/bioinformatics/btaa118.

Brooks, A.S., A.M. Bertoli-Avella, G.M. Burzynski, G.J. Breedveld, J. Osinga, L.G. Boven, J.A. Hurst, G.M.S. Mancini, M.H. Lequin, R.F. de Coo, I. Matera, E. de Graaff, C. Meijers, P.J. Willems, D. Tibboel, B.A. Oostra, and R.M.W. Hofstra. 2005. Homozygous nonsense mutations in KIAA1279 are associated with malformations of the central and enteric nervous systems. *Am. J. Hum. Genet.* 77:120–126. doi:10.1086/431244.

Brouwers, N., N. Mallol Martinez, and I. Vernos. 2017. Role of Kif15 and its novel mitotic partner KBP in K-fiber dynamics and chromosome alignment. *PloS One*. 12:e0174819. doi:10.1371/journal.pone.0174819.

Camera, P., J.S. da Silva, G. Griffiths, M.G. Giuffrida, L. Ferrara, V. Schubert, S. Imarisio, L. Silengo, C.G. Dotti, and F. Di Cunto. 2003. Citron-N is a neuronal Rho-associated protein involved in Golgi organization through actin cytoskeleton regulation. *Nat. Cell Biol.* 5:1071–1078. doi:10.1038/ncb1064.

Capalbo, L., Z.I. Bassi, M. Geymonat, S. Todesca, L. Copoiu, A.J. Enright, G. Callaini, M.G. Riparbelli, L. Yu, J.S. Choudhary, E. Ferrero, S. Wheatley, M.E. Douglas, M. Mishima, and P.P. D'Avino. 2019. The midbody interactome reveals unexpected roles for PP1 phosphatases in cytokinesis. *Nat. Commun.* 10:4513. doi:10.1038/s41467-019-12507-9.

Chalamalasetty, R.B., S. Hümmer, E.A. Nigg, and H.H.W. Silljé. 2006. Influence of human Ect2 depletion and overexpression on cleavage furrow formation and abscission. *J. Cell Sci.* 119:3008–3019. doi:10.1242/jcs.03032.

Dafsari, H.S., S. Byrne, J.-P. Lin, M. Pitt, J.D. Jongbloed, F. Flinter, and H. Jungbluth. 2015. Goldberg-Shprintzen megacolon syndrome with associated sensory motor axonal neuropathy. *Am. J. Med. Genet. A.* 167:1300–1304. doi:10.1002/ajmg.a.36873.

D'Avino, P.P. 2017. Citron kinase - renaissance of a neglected mitotic kinase. *J. Cell Sci.* 130:1701–1708. doi:10.1242/jcs.200253.

Dema, A., F. Macaluso, F. Sgrò, G.E. Berto, F.T. Bianchi, A.A. Chiotto, G. Pallavicini, F. Di Cunto, and M. Gai. 2018. Citron kinase-dependent F-actin maintenance at midbody secondary ingression sites mediates abscission. *J. Cell Sci.* doi:10.1242/jcs.209080.

Di Cunto, F., E. Calautti, J. Hsiao, L. Ong, G. Topley, E. Turco, and G.P. Dotto. 1998. Citron rho-interacting kinase, a novel tissue-specific ser/thr kinase encompassing the Rho-Rac-binding protein Citron. *J. Biol. Chem.* 273:29706–29711.

Donato, V., M. Bonora, D. Simoneschi, D. Sartini, Y. Kudo, A. Saraf, L. Florens, M.P. Washburn, M. Stadtfeld, P. Pinton, and M. Pagano. 2017. The TDH-GCN5L1-Fbxo15-KBP axis limits mitochondrial biogenesis in mouse embryonic stem cells. *Nat. Cell Biol.* 19:341–351. doi:10.1038/ncb3491.

Drerup, C.M., S. Lusk, and A. Nechiporuk. 2016. Kif1B Interacts with KBP to Promote Axon Elongation by Localizing a Microtubule Regulator to Growth Cones. *J. Neurosci. Off. J. Soc. Neurosci.* 36:7014–7026. doi:10.1523/JNEUROSCI.0054-16.2016.

Drévillon, L., A. Megarbane, B. Demeer, C. Matar, P. Benit, A. Briand-Suleau, V. Bodereau, J. Ghoumid, M. Nasser, X. Decrouy, M. Doco-Fenzy, P. Rustin, D. Gaillard, M. Goossens, and I. Giurgea. 2013. KBP-cytoskeleton interactions underlie developmental anomalies in Goldberg-Shprintzen syndrome. *Hum. Mol. Genet.* 22:2387–2399. doi:10.1093/hmg/ddt083.

Eda, M., S. Yonemura, T. Kato, N. Watanabe, T. Ishizaki, P. Madaule, and S. Narumiya. 2001. Rho-dependent transfer of Citron-kinase to the cleavage furrow of dividing cells. *J. Cell Sci.* 114:3273–3284.

Fu, Y., J. Huang, K.-S. Wang, X. Zhang, and Z.-G. Han. 2011. RNA interference targeting CITRON can significantly inhibit the proliferation of hepatocellular carcinoma cells. *Mol. Biol. Rep.* 38:693–702. doi:10.1007/s11033-010-0156-5.

Gai, M., F.T. Bianchi, C. Vagnoni, F. Vernì, S. Bonaccorsi, S. Pasquero, G.E. Berto, F. Sgrò, A.M. Chiotto, L. Annaratone, A. Sapino, A. Bergo, N. Landsberger, J. Bond, W.B. Huttner, and F. Di Cunto. 2016. ASPM and CITK regulate spindle orientation by affecting the dynamics of astral microtubules. *EMBO Rep.* 17:1396–1409. doi:10.15252/embr.201541823.

Gai, M., P. Camera, A. Dema, F. Bianchi, G. Berto, E. Scarpa, G. Germena, and F. Di Cunto. 2011. Citron kinase controls abscission through RhoA and anillin. *Mol. Biol. Cell.* 22:3768–3778. doi:10.1091/mbc.E10-12-0952.

Harding, B.N., A. Moccia, S. Drunat, O. Soukarieh, H. Tubeuf, L.S. Chitty, A. Verloes, P. Gressens, V. El Ghouzzi, S. Joriot, F. Di Cunto, A. Martins, S. Passemard, and S.L. Bielas. 2016. Mutations in Citron Kinase Cause Recessive Microlissencephaly with Multinucleated Neurons. *Am. J. Hum. Genet.* 99:511–520. doi:10.1016/j.ajhg.2016.07.003.

Hirst, C.S., L.A. Stamp, A.J. Bergner, M.M. Hao, M.X. Tran, J.M. Morgan, M. Dutschmann, A.M. Allen, G. Paxinos, T.M. Furlong, S.J. McKeown, and H.M. Young. 2017. Kif1bp loss in mice leads to defects in the peripheral and central nervous system and perinatal death. *Sci. Rep.* 7:16676. doi:10.1038/s41598-017-16965-3.

Hu, C.-K., M. Coughlin, and T.J. Mitchison. 2012. Midbody assembly and its regulation during cytokinesis. *Mol. Biol. Cell.* 23:1024–1034. doi:10.1091/mbc.E11-08-0721.

Janke, C., and G. Montagnac. 2017. Causes and Consequences of Microtubule Acetylation. *Curr. Biol. CB.* 27:R1287–R1292. doi:10.1016/j.cub.2017.10.044.

Jayaraman, D., B.-I. Bae, and C.A. Walsh. 2018. The Genetics of Primary Microcephaly. *Annu. Rev. Genomics Hum. Genet.* 19:177–200. doi:10.1146/annurev-genom-083117-021441.

Jin, M., O. Pomp, T. Shinoda, S. Toba, T. Torisawa, K. Furuta, K. Oiwa, T. Yasunaga, D. Kitagawa, S. Matsumura, T. Miyata, T.T. Tan, B. Reversade, and S. Hirotsune. 2017. Katanin p80, NuMA and cytoplasmic dynein cooperate to control microtubule dynamics. *Sci. Rep.* 7:39902. doi:10.1038/srep39902.

Kawano, Y., Y. Fukata, N. Oshiro, M. Amano, T. Nakamura, M. Ito, F. Matsumura, M. Inagaki, and K. Kaibuchi. 1999. Phosphorylation of myosin-binding subunit (MBS) of myosin phosphatase by Rho-kinase in vivo. *J. Cell Biol.* 147:1023–1038.

Kevenaar, J.T., S. Bianchi, M. van Spronsen, N. Olieric, J. Lipka, C.P. Frias, M. Mikhaylova, M. Harterink, N. Keijzer, P.S. Wulf, M. Hilbert, L.C. Kapitein, E. de Graaff, A. Ahkmanova, M.O. Steinmetz, and C.C. Hoogenraad. 2016. Kinesin-Binding Protein Controls Microtubule Dynamics and Cargo Trafficking by Regulating Kinesin Motor Activity. *Curr. Biol. CB*. 26:849–861. doi:10.1016/j.cub.2016.01.048.

Li, H., S.L. Bielas, M.S. Zaki, S. Ismail, D. Farfara, K. Um, R.O. Rosti, E.C. Scott, S. Tu, N.C. Chi, S. Gabriel, E.Z. Erson-Omay, A.G. Ercan-Sencicek, K. Yasuno, A.O. Çağlayan, H. Kaymakçalan, B. Ekici, K. Bilguvar, M. Gunel, and J.G. Gleeson. 2016. Biallelic Mutations in Citron Kinase Link Mitotic Cytokinesis to Human Primary Microcephaly. *Am. J. Hum. Genet.* 99:501–510. doi:10.1016/j.ajhg.2016.07.004.

Lyons, D.A., S.G. Naylor, S. Mercurio, C. Dominguez, and W.S. Talbot. 2008. KBP is essential for axonal structure, outgrowth and maintenance in zebrafish, providing insight into the cellular basis of Goldberg-Shprintzen syndrome. *Dev. Camb. Engl.* 135:599–608. doi:10.1242/dev.012377.

Macías-Silva, M., S. Abdollah, P.A. Hoodless, R. Pirone, L. Attisano, and J.L. Wrana. 1996. MADR2 is a substrate of the TGFbeta receptor and its phosphorylation is required for nuclear accumulation and signaling. *Cell*. 87:1215–1224.

Mahmood, S., W. Ahmad, and M.J. Hassan. 2011. Autosomal Recessive Primary Microcephaly (MCPH): clinical manifestations, genetic heterogeneity and mutation continuum. *Orphanet J. Rare Dis.* 6:39. doi:10.1186/1750-1172-6-39.

Malaby, H.L.H., M.E. Dumas, R. Ohi, and J. Stumpff. 2019. Kinesin-binding protein ensures accurate chromosome segregation by buffering KIF18A and KIF15. *J. Cell Biol.* 218:1218–1234. doi:10.1083/jcb.201806195.

McKenzie, C., Z.I. Bassi, J. Debski, M. Gottardo, G. Callaini, M. Dadlez, and P.P. D'Avino. 2016. Cross-regulation between Aurora B and Citron kinase controls midbody architecture in cytokinesis. *Open Biol.* 6. doi:10.1098/rsob.160019.

Meng, D., Q. Yu, L. Feng, M. Luo, S. Shao, S. Huang, G. Wang, X. Jing, Z. Tong, X. Zhao, and R. Liu. 2019. Citron kinase (CIT-K) promotes aggressiveness and tumorigenesis of breast cancer cells in vitro and in vivo: preliminary study of the underlying mechanism. *Clin. Transl. Oncol. Off. Publ. Fed. Span. Oncol. Soc. Natl. Cancer Inst. Mex.* 21:910–923. doi:10.1007/s12094-018-02003-9.

Naveed, M., S.K. Kazmi, M. Amin, Z. Asif, U. Islam, K. Shahid, and S. Tehreem. 2018. Comprehensive review on the molecular genetics of autosomal recessive primary microcephaly (MCPH). *Genet. Res.* 100:e7. doi:10.1017/S0016672318000046.

Pagnamenta, A.T., P. Heemeryck, H.C. Martin, C. Bosc, L. Peris, I. Uszynski, S. Gory-Fauré, S. Couly, C. Deshpande, A. Siddiqui, A.A. Elmonairy, WGS500 Consortium, Genomics England Research Consortium, S. Jayawant, S. Murthy, I. Walker, L.

Loong, P. Bauer, F. Vossier, E. Denarier, T. Maurice, E.L. Barbier, J.-C. Deloulme, J.C. Taylor, E.M. Blair, A. Andrieux, and M.-J. Moutin. 2019. Defective tubulin detyrosination causes structural brain abnormalities with cognitive deficiency in humans and mice. *Hum. Mol. Genet.* 28:3391–3405. doi:10.1093/hmg/ddz186.

Pallavicini, G., G. Iegiani, G.E. Berto, E. Calamia, E. Trevisiol, A. Veltri, S. Allis, and F. Di Cunto. 2020. CITK Loss Inhibits Growth of Group 3 and Group 4 Medulloblastoma Cells and Sensitizes Them to DNA-Damaging Agents. *Cancers*. 12. doi:10.3390/cancers12030542.

Pallavicini, G., F. Sgrò, F. Garello, M. Falcone, V. Bitonto, G.E. Berto, F.T. Bianchi, M. Gai, A.M.A. Chiotto, M. Filippi, J.C. Cutrin, U. Ala, E. Terreno, E. Turco, and F.D. Cunto. 2018. Inactivation of Citron Kinase Inhibits Medulloblastoma Progression by Inducing Apoptosis and Cell Senescence. *Cancer Res.* 78:4599–4612. doi:10.1158/0008-5472.CAN-17-4060.

Passemard, S., A.M. Kaindl, and A. Verloes. 2013. Microcephaly. *Handb. Clin. Neurol.* 111:129–141. doi:10.1016/B978-0-444-52891-9.00013-0.

Pilaz, L.-J., J.J. McMahon, E.E. Miller, A.L. Lennox, A. Suzuki, E. Salmon, and D.L. Silver. 2016. Prolonged Mitosis of Neural Progenitors Alters Cell Fate in the Developing Brain. *Neuron*. 89:83–99. doi:10.1016/j.neuron.2015.12.007.

Salvetti, A., Y. Couté, A. Epstein, L. Arata, A. Kraut, V. Navratil, P. Bouvet, and A. Greco. 2016. Nuclear Functions of Nucleolin through Global Proteomics and Interactomic Approaches. *J. Proteome Res.* 15:1659–1669. doi:10.1021/acs.jproteome.6b00126.

Sgrò, F., F.T. Bianchi, M. Falcone, G. Pallavicini, M. Gai, A.M.A. Chiotto, G.E. Berto, E. Turco, Y.J. Chang, W.B. Huttner, and F. Di Cunto. 2016. Tissue-specific control of

midbody microtubule stability by Citron kinase through modulation of TUBB3 phosphorylation. *Cell Death Differ.* 23:801–813. doi:10.1038/cdd.2015.142.

Valence, S., K. Poirier, N. Lebrun, Y. Saillour, P. Sonigo, B. Bessières, T. Attié-Bitach, A. Benachi, C. Masson, F. Encha-Razavi, J. Chelly, and N. Bahi-Buisson. 2013. Homozygous truncating mutation of the KBP gene, encoding a KIF1B-binding protein, in a familial case of fetal polymicrogyria. *Neurogenetics*. 14:215–224. doi:10.1007/s10048-013-0373-x.

Woods, C.G., and A. Parker. 2013. Investigating microcephaly. *Arch. Dis. Child.* 98:707–713. doi:10.1136/archdischild-2012-302882.

Wozniak, M.J., M. Melzer, C. Dorner, H.-U. Haring, and R. Lammers. 2005. The novel protein KBP regulates mitochondria localization by interaction with a kinesin-like protein. *BMC Cell Biol.* 6:35. doi:10.1186/1471-2121-6-35.

Zhou, X., Y. Zhi, J. Yu, and D. Xu. 2020. The Yin and Yang of Autosomal Recessive Primary Microcephaly Genes: Insights from Neurogenesis and Carcinogenesis. *Int. J. Mol. Sci.* 21. doi:10.3390/ijms21051691.

Materials and methods

Cell culture and synchronization.

Unmodified HeLa cells were originally obtained from ATCC and a new batch was thawed after 5 passages. All cells are routinely screened for mycoplasma contamination. HeLa cells were cultured in RPMI medium supplemented with 10% fetal bovine serum (FBS) and 1% penicillin/ streptomycin. The HeLa cell line expressing α-tubulin–GFP was maintained in DMEM-GlutaMAX (Invitrogen) supplemented with 10% FBS, 100 U ml−1 penicillin, 100 µg ml−1 streptomycin, 200 µg ml−1 Geneticin (Sigma, St Louis, MO, USA) and 0.5 µg

ml−1 puromycin. All cells were cultured in a humidified 5% CO2 incubator at 37°C. For synchronization, asynchronous cultures were supplemented with 25 µg/ml Aphidicolin (Sigma) and maintained under these conditions for 24 h and then cultured for a further 16 h in fresh complete medium in the presence of 50 ng/ml nocodazole (Sigma) to block cells at prometaphase. Finally, cells were washed three times with fresh medium and allowed to progress through mitosis/cytokinesis for the indicated times.

HEK293T cells were cultured in DMEM supplemented with 10% fetal Calf serum (FCS) and 1% penicillin/streptomycin (Life Technologies, ThermoFisher, Waltham, MA). For both cell lines, the number of in vitro passages from thawing of the original aliquots to experiments was comprised between 5 and 8. Cells were routinely analyzed for morphological features and tested for Mycoplasma contamination with the following oligonucleotides sequences: MYCO1 5'-ACTCCTACGGGAGGCAGCAGTA-3'; MYCO2: 5'-TGCACCATCTGTCACTCTGTTAACCTC-3'.

Transfection RNAi and constructs.

Previously published CITK double-stranded RNAs were used (Gai et al., 2011). For knockdown of KIF1BP KIA1269 ONTARGETplus Dharmacon SMART pools were used. D-001810-10 non-targeting pool was used as a negative control (Dharmacon, Lafayette, CO). HeLa cells plated on six-well plates were transfected using 6.25 µl of the required siRNA (20 µM) together with 1.5µL Lipofectamine 2000 (Invitrogen, Carlsbad, CA), according to the manufacturer's instructions. HEK293T cells were transfect by Home-made CaCl2. CITK Cherry -tagged and Myc-tagged constructs used in this manuscript were previously published (Gai et al., 2011). FLAG-tagged and GFP tagged KIF1BP constructs were kindly provided from Pagano Lab (Donato et al., 2017).

Immunoprecipitations and western blotting.

For all immunoprecipitations, cells were extracted with lysis buffer containing 150 mM NaCl, 1 mM MgCl2, 50 mM Tris pH 7, 1% NP40, 5% Glycerol protease inhibitors (Roche,

Basel; Switzerland) and 1mM phenylmethylsulfonyl fluoride (PMSF). Antibodies and Dynabeads protein G (GE Healthcare Life Science, Little Chalfont, UK) were added to cleared lysates and incubated for 2 hours at 4°C. Pellets were washed four times with lysis buffer and analyzed by SDS-PAGE. For immunoblots and immunoprecipitates equal amounts of proteins from total cell lysates were resolved by reducing SDS-PAGE and transferred to nitrocellulose filters that were then incubated with the indicated antibodies.

MS-based proteomic analyses

Eluted proteins were stacked in the top of a SDS-PAGE gel (4-12% NuPAGE, Life Technologies), stained with Coomassie blue R-250 (Bio-Rad) before in-gel digestion using modified trypsin (Promega, sequencing grade) as previously described (Salvetti et al., 2016). Resulting peptides were analyzed by online nanoliquid chromatography coupled to tandem MS (UltiMate 3000 and LTQ-Orbitrap Velos Pro, Thermo Scientific). Peptides were sampled on a 300 µm x 5 mm PepMap C18 precolumn and separated on a 75 µm x 250 mm PepMap C18 column (Thermo Scientific) using a 120-min gradient. MS and MS/MS data were acquired using Xcalibur (Thermo Scientific). Peptides and proteins were identified using Mascot (version 2.6) through concomitant searches against Uniprot database (*Homo sapiens* taxonomy), classical contaminant database (homemade) and the corresponding reversed databases. The Proline software (Bouyssié et al., 2020) was used to filter the results: conservation of rank 1 peptides, peptide score ≥ 25, peptide length ≥ 6 amino acids, peptide-spectrum-match identification false discovery rate < 1% as calculated on scores by employing the reverse database strategy, and minimum of 1 specific peptide per identified protein group. Proline was then used to perform a compilation, grouping and spectral counting-based comparison of the protein groups identified in the different samples. Proteins from the contaminant database and additional keratins were discarded from the final list of identified proteins. To be considered as a potential CITK interactor, a protein must be identified in CITK, CITN or CITKD eluates with a minimum of three specific

spectral counts and not in negative control eluate, or enriched at least 10 times in CITK, CITN or CITKD eluates compared to negative control eluate.

Immunofluorescence.

Cells were fixed methanol at –20°C for 10 min, saturated in 5% BSA in PBS for 30 min and incubated with a primary antibody for 1h at RT. Primary antibodies were detected with anti-rabbit Alexa Fluor 488 or 568 (Molecular Probes, Invitrogen), anti-mouse Alexa Fluor 488 or 568 (Molecular Probes, Invitrogen) used at 1:1000 dilution for 30 min. Cells were counterstained with 0.5 µg/mL DAPI for 10 min and washed with PBS.

Antibodies

The following antibodies were used: mouse monoclonal anti-Citron (#611377 Transduction Laboratories, BD Biosciences, San Jose, CA, USA), rabbit polyclonal anti-KIF1BP (#NBP1-84143,Novus Biologicals, Colorado, USA), mouse monoclonal anti-KIF1BP (H12) for endogenous immune precipitation (#sc-390449 Santacruz, Dallas, TX, USA), rabbit polyclonal anti-βactin (#A2066 Sigma-Aldrich), mouse anti FLAG (#F3165 Sigma-Aldrich),mouse anti Myc TAG (#05-419 Sigma-Aldrich), RFP-Trap Magnetic Agarose (#rtma-10 Chromotek, Planegg, Germany) for immunoprecipitation of Cherry-tagged proteins and mouse monoclonal home-made mCherry for blots, mouse monoclonal anti-AURKB (#A78720, Transduction Laboratories, BD Biosciences, San Jose, CA, USA), rabbit polyclonal anti-INCENP (#2807, Cell Signalling Technology, Danvers, MA, USA),), rabbit polyclonal anti-tyrosinated tubulin (#ABT171 Sigma-Aldrich), mouse anti-acetylated tubulin (#T6199 Sigma-Aldrich) and mouse anti-tubulin (#T5168 Sigma-Aldrich).

Microscopy

Imaging was performed using a Leica TCS SP5 confocal system (Leica Microsystems) equipped with a 405 nm diode, an argon ion, a 561 nm DPSS and a HeNe 633 nm lasers. Fixed cells were imaged using a HCX PL APO 63×/1.4 NA oil immersion objective. For live imaging, time lapses were recorded overnight with an interval of 5 min using a 40×

PlanApo N.A. 1.4 oil immersion objective on the cells kept in the microscope incubator at 37°C and 5% CO2. Super-resolution images were obtained using a Leica SP8 confocal system with HyVolution 2 (Leica Microsystems) equipped with an argon ion, a 561 nm DPSS and a HeNe 633 nm lasers. Fixed cells were imaged using a HCX PL APO 63×/1.4 NA oil immersion objective. Series of x-y-z images (typically 0.04×0.04×0.106 µm3 voxel size) were collected.

Statistical analysis

Statistical analyses were performed using Microsoft Office Excel or Graphpad. The mean values shown represent the average of at least three independent experiments and error bars are standard errors of the mean.

Figures and legends

Figure 1. Biochemical analysis of KIF1BP/CITK interaction.

(A) Western blot analysis, with the indicated antibodies, of total cell lysates and RFP-Trap-based immunoprecipitations, obtained from 293-T cells transfected with constructs expressing the indicated Cherry-tagged proteins or with empty control vector.

(B) Western blot analysis, with the indicated antibodies, of total cell lysates and anti-Myc immunoprecipitations, obtained from 293-T cells transfected with pcDNA3.1 vector (empty) or with vectors expressing the indicated Myc-tagged CITK proteins.

(C) Western blot analysis, with the indicated antibodies, of total cell lysates and anti-FLAG immunoprecipitations, obtained from 293-T cells transfected with pCag vector (empty) or pCag expressing FLAG-KIF1BP, in combination with vectors expressing MYC-tagged CITK proteins.

(D) Western blot analysis, with the indicated antibodies, of total cell lysate and immunoprecipitation with control (α-Ig) and anti-KIF1BP, from HeLa synchronized in mitosis, lysed 30 min after nocodazole release.

Figure 2. KIF1BP localizes at the midbody and its knockdown leads to cytokinesis failure.

(A) Immunostaining for Tubulin and KIF1BP of HeLa cells midbodies, 96 hours after treatment with non-targeting (siCtrl) or KIF1BP-specific (siKIF1BP) siRNA sequences. Scale bars = 5 µm

(B) High magnification of midbodies of HeLa cells transfected with GFP-KIF1BP and immunostained for Tubulin and GFP 48 hours after transfection. Scale bars = 5 µm

(C) Total cell lysates from HeLa cells, treated for 96 hours with non-targeting (siCtrl) or KIF1BP-specific (siKIF1BP) siRNA sequences were analyzed with anti KIF1BP. Internal loading control was Vinculin (VINC).

(D) HeLa cells, seeded at low density, were processed for immunofluorescence 96 hours after transfection with non-targeting (siCtrl) or KIF1BP-specific (siKIF1BP) siRNA sequences, and stained with DAPI and anti-alpha-tubulin antibodies. The percentage of binucleated cells was then assessed.

(E) HeLa cells, seeded at low density, were analyzed overnight by live cell imaging, 84 hours after transfection with non-targeting (siCtrl) or KIF1BP-specific (siKIF1BP) siRNA sequences. Scale bars = 10 µm

(F) Quantification of cells, analyzed as in panel C, that reach anaphase but fail cytokinesis The intensity plots shown in A and B were determine along a 10 µm line centered on midbody dark zone. All quantifications were based on at least 4 independent biological replicates. Error bars = standard error of the mean. *** $P < 0.001$, Chi-square test.

Figure 3. KIF1BP and CITK localize at the midbody.

(A) Immunostaining for Tubulin and KIF1BP of HeLa cells midbodies, 48 hours after treatment with non-targeting (siCtrl) or CITK-specific (siCITK) siRNA sequences.

(B) Quantification of KIF1BP intensity at midbody of cells treated as in panel B.

(C) Tubulin and CITK immunostaining of HeLa midbodies, after treatment for 96 hours with non-targeting (siCtrl) or KIF1BP-specific (siKIF1BP) siRNA sequences. Scale bars = 5 µm

(D) Quantification of CITK intensity at midbody of cells treated as in panel E.

All scale bars = 5 µm. All quantifications were based on at least 5 independent biological replicates, unless noted otherwise. Error bars = standard error of the mean. ** $P < 0.01$, two tailed Student's T-test.

Figure 4. KIF1BP knockdown increases the proportion of unstable microtubules at midbody and impairs CPC localization

(A) HeLa cells, seeded at low density, were processed for immunofluorescence 96 hours after transfection with non-targeting (siCtrl) or KIF1BP-specific (siKIF1BP) siRNA sequences, and stained with DAPI, anti-tyrosinated and anti-acetylated tubulin antibodies. Scale bars = 10 µm

(B) Ratio of acetylated tubulin to tyrosinated tubulin at intercellular bridge of cells treated as in panel A.

(C) High magnification of HeLa treated for 96 hours with non-targeting (siCtrl) or KIF1BP-specific (siKIF1BP) siRNA sequences, stained with anti-Tubulin and anti-AURKB antibodies. Scale bars = 5 µm

(D) Quantification of AURKB midbody intensity and of midbodies with mis-localized AURKB, in cells treated as in panel C.

(E) High magnification of HeLa treated for 96 hours with non-targeting (siCtrl) or KIF1BP-specific (siKIF1BP) siRNA sequences, stained with anti-Tubulin and anti-INCENP. Scale bars = 5 µm

(F) Quantification of INCENP midbody intensity and of midbodies with mis-localized INCENP, in cells treated as in panel E.

All quantifications were based on at least 3 independent biological replicates, unless noted otherwise. Error bars = standard error of the mean. * $P < 0.05$, *** $P < 0.001$, two tailed Student's T-test for intensity quantification, Chi-square test for localization's percentage.

Figure S1. Silver stain of SDS-PAGE of immune-complexes

(A)Silver stain of SDS-PAGE of immunocomplexes obtained by RFPTRAP of 293 lysate transfected for 48h with Cherry (35KDa) or cherry tagged CITN (180KDa), CITK and CITKD (220 KDa).

Figure 1

Pallavicini G. et al.

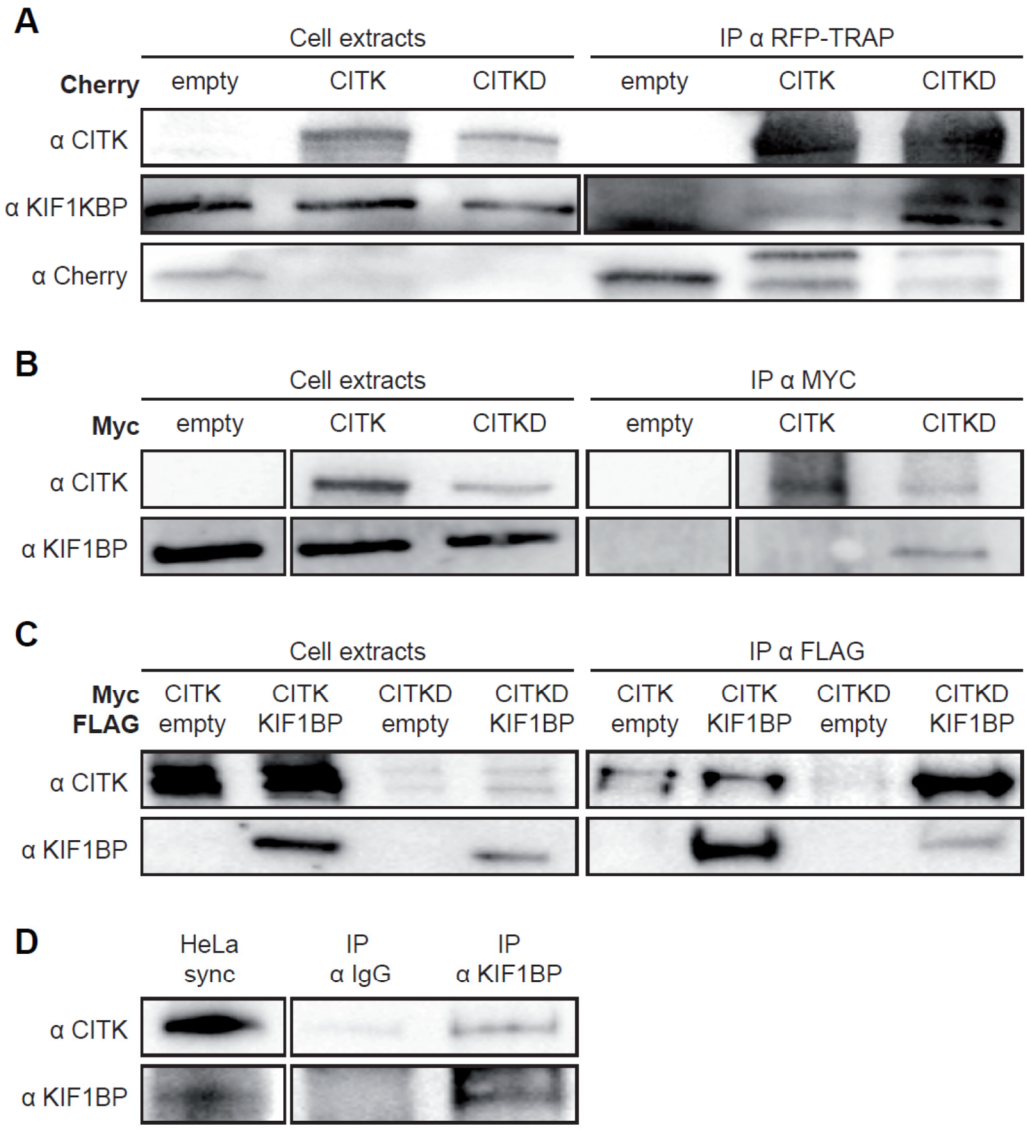

Figure 2

Pallavicini G. et al.

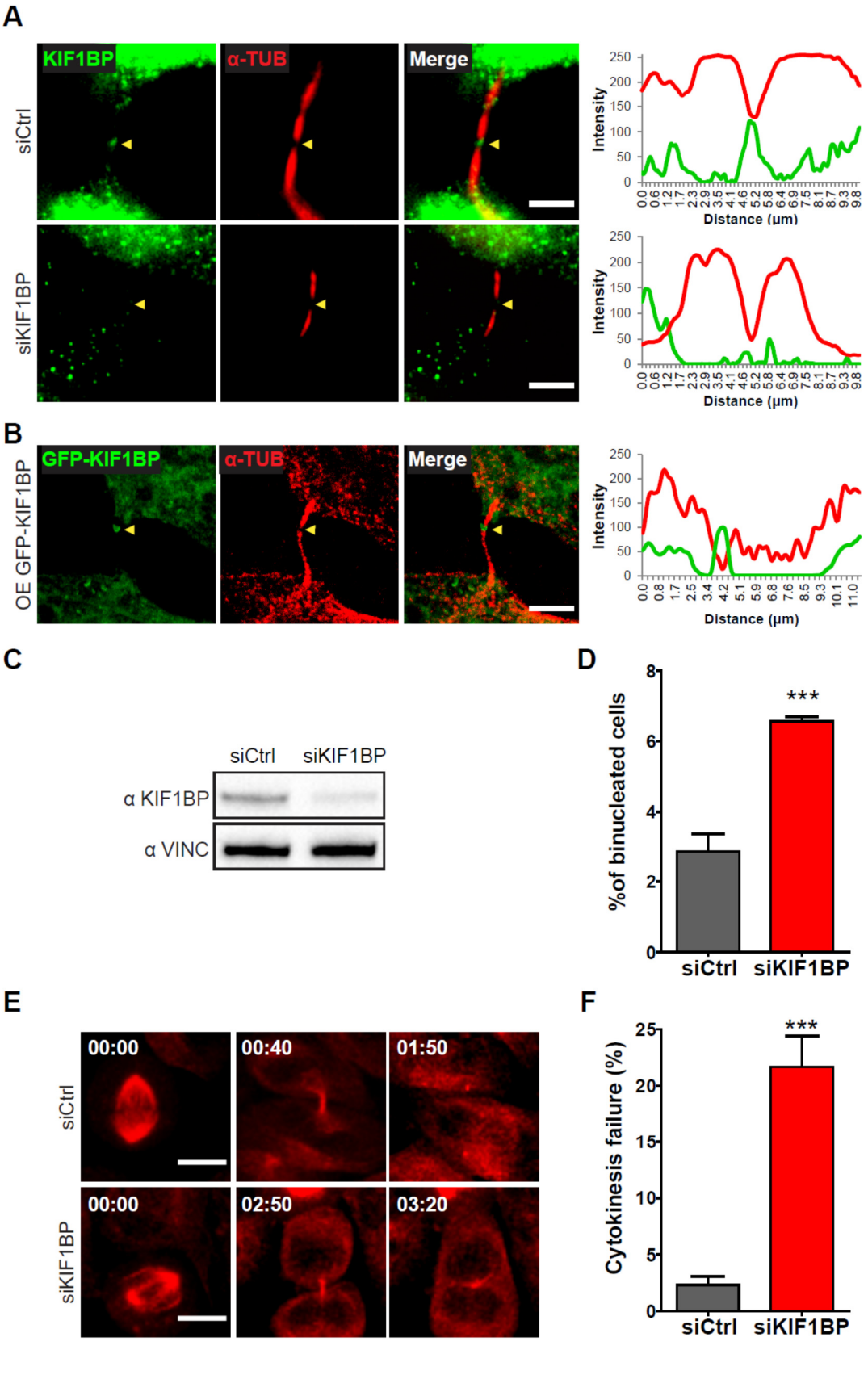

Figure 3

Pallavicini G. et al.

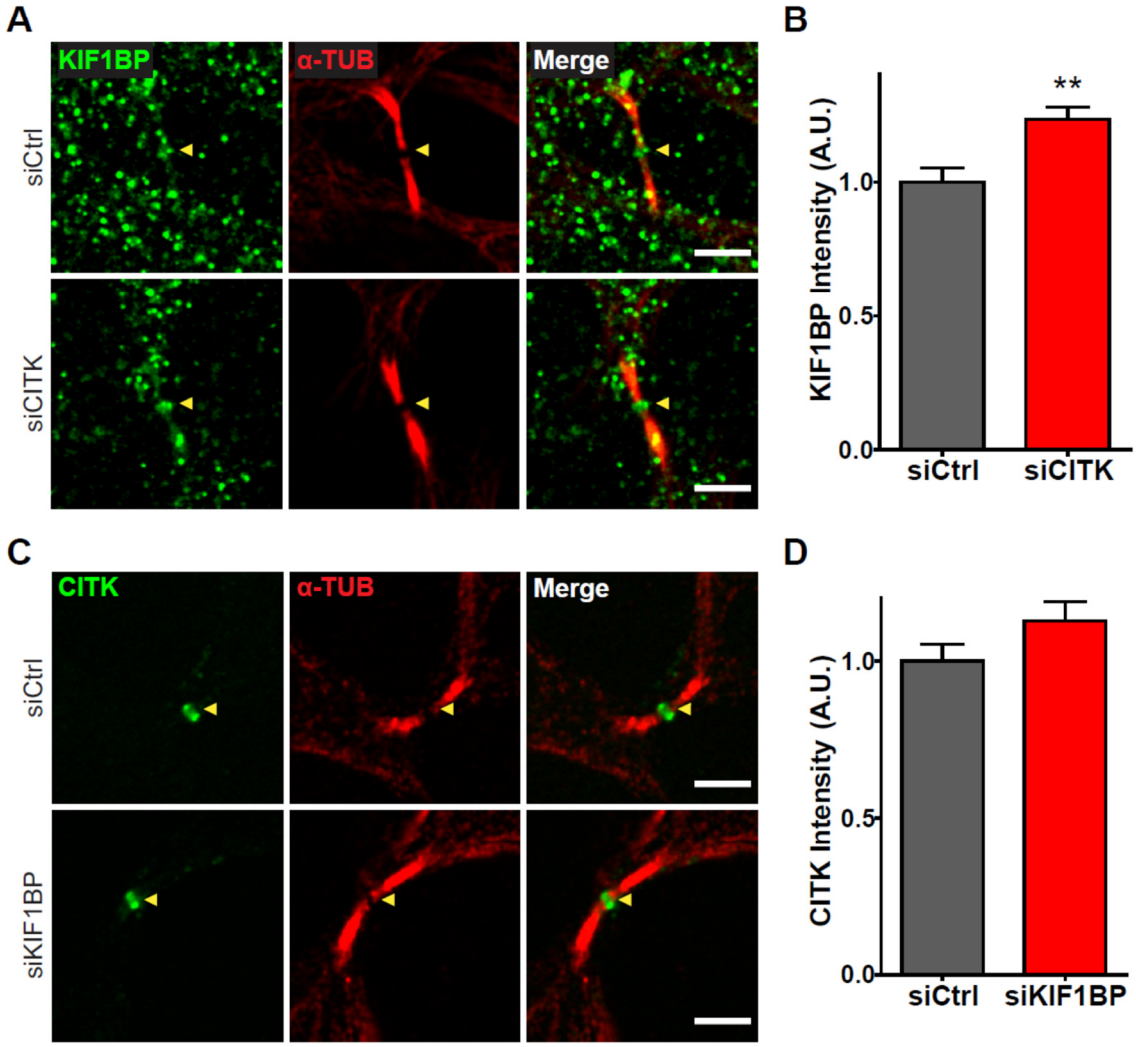

Figure 4

Pallavicini G. et al.

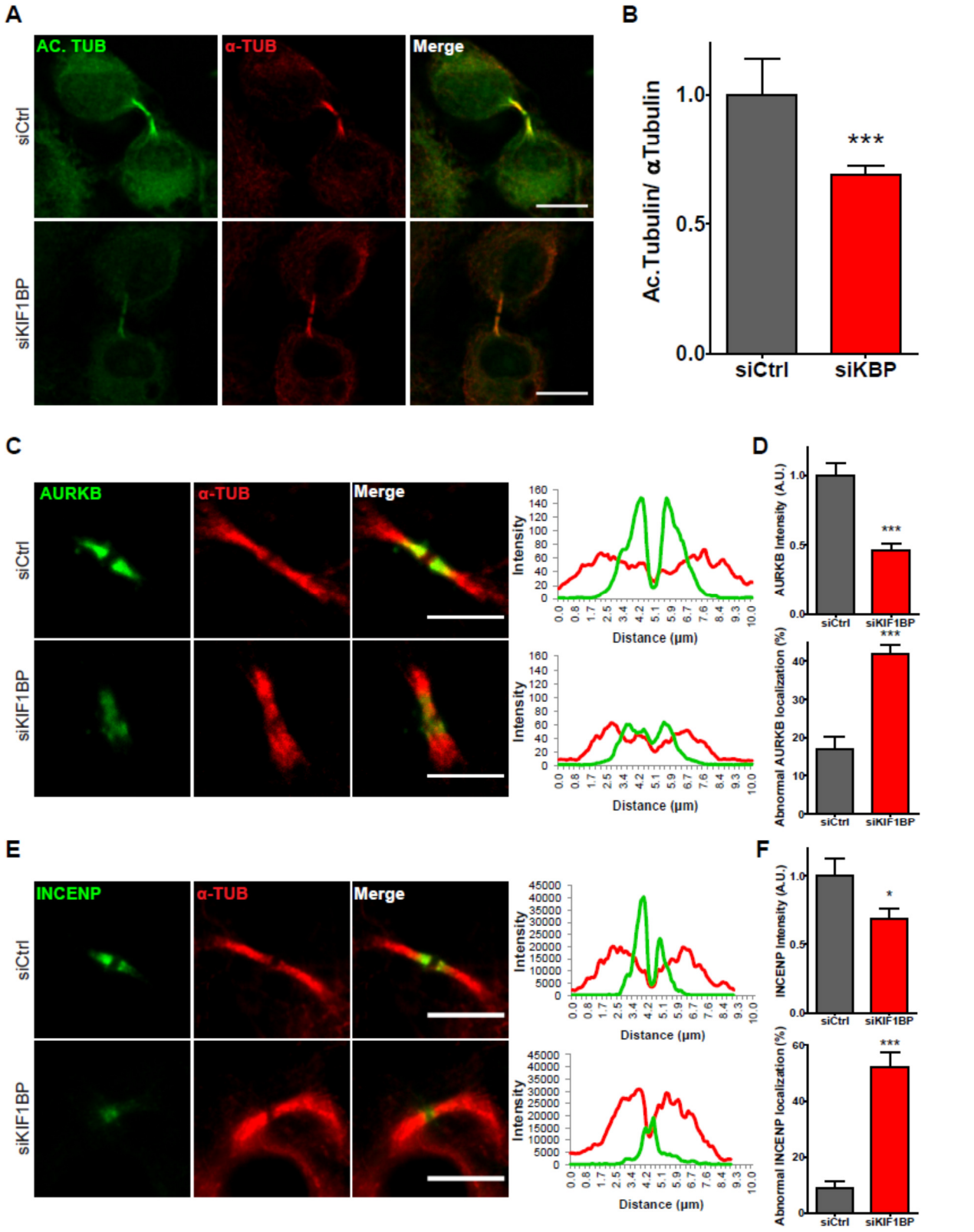

Figure S1

Pallavicini G. et al.